energy&fuels

Article

pubs.acs.org/EF

Parametric Characterization of Air Gasification of *Chlorella vulgaris* Biomass

Abdul Raheem,[†] Valerie Dupont,[‡] Abdul Qadir Channa,[§] Xiao Zhao,[†] Arun K. Vuppaladadiyam,[†] Yun-Hin. Taufiq-Yap,[∥] Ming Zhao,*[,†,⊥] and Razif Harun*[,#]

[†]School of Environment, Tsinghua University, Beijing 100084, China

[‡]School of Chemical and Process Engineering, The University of Leeds, Leeds, LS2 9JT, U.K.

[§]Department of Mechanical Engineering, Vocational Training Center, Khairpur (Mir's), Sindh 66020, Pakistan

[∥]Catalysis Science and Technology Research Centre, Faculty of Science, and [#]Department of Chemical and Environmental Engineering, Universiti Putra Malaysia, 43400 Serdang, Malaysia

[⊥]Key Laboratory for Solid Waste Management and Environment Safety, Ministry of Education, Beijing, 100084, China

ABSTRACT: The gasification of green algae *Chlorella vulgaris* in air was investigated using both a thermogravimetric analyzer (TGA) and a bench scale horizontal axis quartz tube reactor (HQR). The full range of solid state kinetic models produced best fits with TGA results varied for the five subzones of conversion vs temperature, with the nucleation and nuclei growth "A2" followed by "A3" or contracting volume models producing close matches for $T \leq 367$ °C, a zero-order model between 358 and 468 °C, and contracting surface models for $T \geq 458$ °C; each model yielding their set of apparent activation energy ($E < 41$ kJ mol^{-1}) and pre-exponential factors ($A > 0.04$ s^{-1}) corresponding to rate constants in the range 0.001−0.005 s^{-1}. The HQR was used to investigate the effects of microalgal biomass loading, temperature, and equivalence ratio (ER) on C_nH_m/CO/H_2 gas yield and composition, carbon conversion efficiency (CCE), and lower heating value (LHV) of syngas under air gasification conditions. Increasing microalgal biomass loading from 1 to 2 g led to a decrease in H_2 content (24.2−19.5 vol %) in the gases. An optimal temperature of 950 °C resulted in the highest H_2, CO, and CH_4 yields at 2.9, 22.8, and 10.1 wt % of biomass from a maximum gas yield of 76.1 wt %, and highest H_2/CO ratio (1.75) and CCE of 56.3%. The effect of ER was measured in two phases 0.1−0.26 and 0.26−35, respectively. During the first phase, the positive effect of ER played a major part compared to second phase, so the H_2 content, H_2 yield, CCE, and LHV were increased.

1. INTRODUCTION

Synthesis gas (syngas) is considered as an environmental friendly fuel with high potential for commercial applications such as transportation, heat, and electricity generation via fuel cells in near future.[1,2] Currently, the majority of syngas at industrial scale is supplied from fossil fuels, mostly from coal gasification and natural reforming processes.[3] The high reliance on these resources produces large amounts of carbon dioxide (CO_2) and hence increases the greenhouse gaseous concentration in the atmosphere.[4,5] Also, issues related to fossil fuels as well as the increasing social and industrial awareness of their environmental drawbacks have created the need to promote more sustainable alternative resources for syngas production. Bioenergy presently provides roughly 10% of global supplies.[6,7]

Biomass-derived syngas appears to be a promising fuel for transportation, fuel cells for electricity generation, and other stationary applications.[8] Although various biomasses have been extensively utilized to produce syngas, the utilization of the feedstock may have a series of issues related to arable land usage particularly for food production and other high value products and technical obstacles for product conversion; these make syngas production economically less appealing.[9] Moreover, these biomasses are lignocellulosic, causing key downstream conflicts in the removal or conversion of remaining lignin to support and maximize the synthesis gas conversion and production competences.[10,11]

Microalgae are a renewable cellular feedstock for biofuel production, which offer several advantages such as the ability to accumulate a high quantity of protein, carbohydrates, and lipid, semisteady state production, suitability to be grown in a variety of climate conditions, absence of lignin, high calorific value, and low density, as well as low viscosity.[12,13] The above benefits provide microalgae with a suitable capacity to substitute current syngas production commodities. Thermochemical gasification is a well-established technology to convert biomass into gaseous products and categorized depending on the gasifying agent such as air, steam, O_2-enriched air, etc. Thermochemical gasification converts biomass residues into a syngas under partial oxidation mainly including H_2, CO, CO_2, and CH_4. Syngas is primarily suitable for power generation and heat. It can also be utilized as an intermediate resource to produce hydrogen, industrial chemicals, ammonia, and transportation fuels via chemical (syngas catalytic reforming) and biological processes (syngas fermentation).[14,15] However, the quality and quantity of syngas are highly dependent on the feedstock composition, gasifier design, and process parameters such as biomass loading, temperature, gasifying agent, and equivalence ratio.

To mark algal biomass as a future sustainable fuel, the potential of microalgae for syngas production have been

Received: December 27, 2016
Published: February 13, 2017

DOI: 10.1021/acs.energyfuels.6b03468
Energy Fuels 2017, 31, 2959−2969

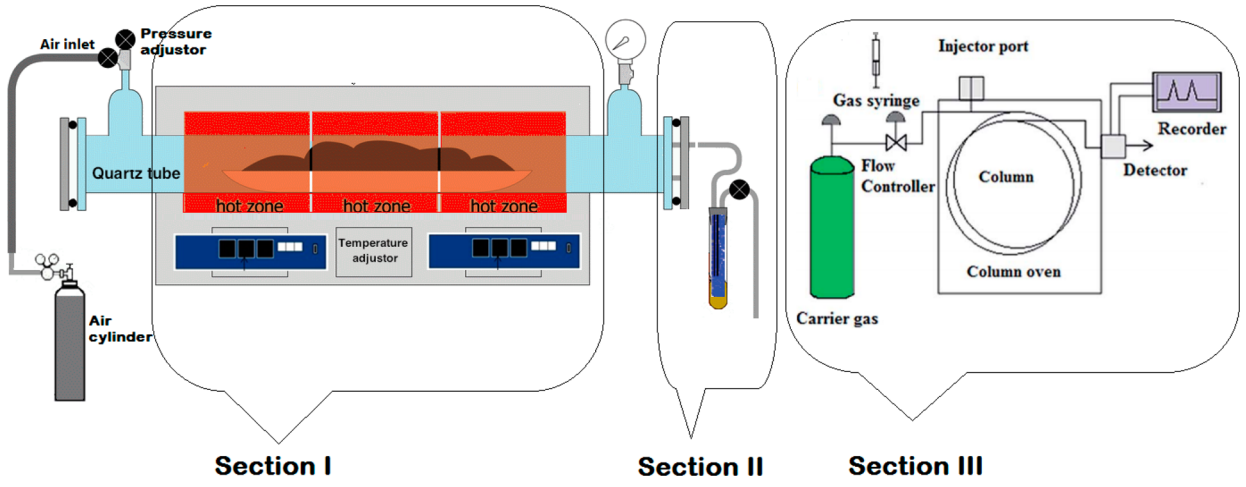

Figure 1. Schematic diagram of the horizontal axis quartz tube reactor (HQR).

assessed via hydrothermal and supercritical water gasification.[16−19] These typically investigate the process parameters influencing microalgal syngas production. Only limited research highlighting dry gasification of algal biomass has been published for syngas production. Hirano et al.[20] partially gasified a *Spirulina* sp. at 850 to 1000 °C with a constant feeding rate of 0.25 g min^{-1}. The syngas primarily consisted of CO, H_2, CO_2, and CH_4. The temperature played an important role leading to an increase in H_2 contents, while CO, CO_2, and CH_4 decreased. The carbon conversion was also increased from 93% to 100% with increase in temperature from 850 to 1000 °C. Minowa et al.[21] gasified *C. vulgaris* biomass under a nitrogen cycling system in the presence of a Ni-catalyst at 350 °C. The addition of catalyst into the gasification system favored more CH_4 production than H_2 production. However, carbon conversion efficiency and gas yield were increased with catalyst loading.

Vertical, fixed, and fluidized bed gasifiers are used for microalgal gasification.[22−24] However, these reactors encounter challenges in regard to loss of carbon and scalability which makes the reactors less feasible for commercial-scale applications.[25] In comparison, a horizontal reactor configuration is advantageous by intensifying the biomass contact time and improving transfer of heat due to a heavy particle−metal surface interaction and producing a smaller amount of tar compared to the current vertical designs. Moreover, the horizontal axis quartz tube reactor (HQR) provides simple operation, easy control of reaction conditions, and higher carbon conversion rate.[26,27]

On the basis of our knowledge, published studies on microalgae dry gasification have never considered HQR and air as a gasifying agent except for our previous work.[28] The study of the HQR gasification, thermogravimetric behavior (TGA-DTG) as a function of mass conversion under air stream, and kinetic modeling will be useful in regulating, optimizing, and advancing industrial processes.

This research thus explores the microalgal gasification using an HQR and air as a gasifying agent (air is advantageous compared to other gasifying agents such as steam and pure oxygen, those makes the whole process lengthy, complex, and costly) under different treatment specifications including microalgal biomass loading, reactor temperature, and equivalence ratio to investigate their effects on product distribution, C_nH_m + CO + H_2 gas composition, lower heating value of syngas, and carbon conversion efficiency (CCE). Thermogravimetric characteristics, kinetic modeling, and a reduced number of independent, global gasification reactions were postulated in order to best describe the devoltization behavious and yields of char (assumed $C_{(S)}$) and gases obtained. The results obtained from this study will facilitate exploitation of *C. vulgaris* potential for sygans production, which may eventually promote its industiral scale production.

2. EXPERIMENTAL SECTION

2.1. Biomass Sample. *Chlorella vulgaris* (green microalgae) biomass obtained from PureBulk Innc (USA) was used for gasification purpose in this study. The biomass was supplied in a dried powder form with an average size of 100 μm. The biomass is an intact cell where all the compounds are still entrapped in the cell wall. The powder was used as received and stored in a desiccator until further analysis.

2.2. Ultimate Analysis of the *C. vulgaris* and Higher Heating Value. The ultimate analysis of the microalgae sample was conducted and the C, H, N, and S content of *C. vulgaris* was determined using a CHNS analyzer (LECO True Spec CHNS628, USA). The oxygen content was measured by the balance via eq 1. The higher heating value (HHV) of the sample was measured based on Dulong formula[29] eq 2 using sample's elemental composition (see Table 2).

$$\text{O wt \%} = 100\ \text{wt \%} - \text{C wt \%} - \text{H wt \%} - \text{N wt \%} - \text{S wt \%} \quad (1)$$

$$\text{HHV} = 33.86\text{C} + 144.4 \times \left(\text{H} - \frac{\text{O}}{8}\right) + 9.428\text{S} \quad (2)$$

2.3. Thermogravimetric (TG) Analysis. TG/DTG (thermal gravity/differential thermal analysis) combined with a thermal analyzer (Mettle Toledo, SDTA851/SF, USA) was used to study the thermal stability and gasification characteristics of the microalgae biomass. The tests were performed in air atmosphere with flow rate of 25 mL min^{-1}. The analysis temperature was raised from ambient temperature to 1000 °C at heating rate of 10 and 20 °C min^{-1}. The mass of sample used was 20 ± 2 mg.

2.4. Biomass Gasification. The gasification of microalgal biomass was carried out using a horizontal axis quartz tube reactor (HQR). The investigated parameters were microalgal biomass loading, temperature, and ER. The levels of these

DOI: 10.1021/acs.energyfuels.6b03468
Energy Fuels 2017, 31, 2959−2969

variables are the ranges/values at which the experiments were being executed. The investigated ranges include: microalgal biomass loading (0.3, 0.6, 1.0, 1.5, and 2 g), temperature (700, 750, 800, 850, 900, 950 °C), and ER (0.1, 0.2, 0.26, 0.3, 0.35).

2.5. Experimental Facility and Procedure. The HQR used in this study is shown in Figure 1. The gasification specifications were input in a computer to trigger the furnace operation at different test conditions. Four steps were followed to operate the reactor: (i) Prior to each experiment, the reactor was cleansed with N_2 at a flow rate of 10 mL min^{-1} for 10 min to eliminate entrapped gas molecules and (ii) fed with desired biomass (*C. vulgaris*). (iii) Preferred temperatures were attained. (iv) The reaction was also stabilized for desired holding time before completion. The experimental characteristics comprise three key sections: (I) the reactor, (II) the gas cleaning section, and (III) the dry gas sampling and analysis section. The HQR is made of quartz tube and is heated up by the electrical furnace equipped with a K-type thermocouple that was connected to a temperature controller. A sampling boat was used to feed biomass sample inside the reactor with varying concentration and different process conditions (e.g., heating rate, temperature etc.). Air was used as the gasifying agent. Air was continuously flowing in the reactor throughout the whole duration of the experiments. After attaining the desired furnace temperature, it was stabilized/held at the same temperature for 20 min for each experiment, termed "holding time", and after 20 min the furnace was shut down. The gaseous products flowed out of the reactor and passed through the gas cleaning section. Subsequently the cleaned gas stream accumulated in gas sampling bag throughout the whole duration of the experiment. Sample bag contents were then analyzed off line through gas chromatography (GC). The reactor was left to be cooled down to desired temperature in order to collect the solid residues and tar. Solid residue and tar were collected in separate glass bottles and weighted, which were then recorded as char and tar fractions directly.

2.6. Method of Gas Sampling and Analysis. Main gas components such as hydrogen (H_2), carbon monoxide (CO), carbon dioxide (CO_2), and methane (CH_4) were characterized using GC (Model Agilent 6890N; G 1540N), which functioned based on a thermal conductivity detector (TCD) with Varian capillary (HP-PLOT/Q) and molecular sieve (HP-MOLSIV) columns. The TCD was calibrated using a standard gas (Air Products, Singapore) mixture containing CO_2, CO, CH_4, H_2, and He. The total gas composition of four variables was considered 100% and expressed in volume percent. Helium was used as carrier gas.

2.7. Methods of Data Processing. To evaluate the process technology, the following variables were determined:

(a) The lower heating values (LHV, MJ N m^{-3}) of the gaseous products were calculated based on the concentration of H_2, CO, and CH_4 (i.e., these components have combustion value) using eq 3.[30]

$$\begin{aligned}&\mathrm{LHV(MJ\,N\,m^{-3})}\\&= (\mathrm{H_2(vol\,\%)} \times 107.98 + \mathrm{CO(vol\,\%)} \times 126.36\\&\quad + \mathrm{CH_4(vol\,\%)} \times 358.18)/1000\end{aligned} \tag{3}$$

(b) The yield of produced gas was calculated by eq 4

$$\begin{aligned}&\mathrm{yield(mg\,g\ biomass^{-1})}\\&= (\mathrm{H_2,\ CO,\ CO_2,\ and\ CH_4\ produced\ (g)})\\&\quad \times 1000/\mathrm{total\ gas\ produced\ (g)}\end{aligned} \tag{4}$$

(c) Equivalence ratio (ER)

$$\mathrm{ER} = \frac{(\dot{m}_{\mathrm{air}} \times \Delta t_{\mathrm{hold}})/\dot{m}_{\mathrm{biomass}}}{[(m_{\mathrm{air}})/m_{\mathrm{biomass}}]_{\mathrm{stoichiometric}}} \tag{5}$$

where, m denotes mass, $\dot{m}$ is mass flow rate, and Δt_{hold} is the holding time. Section 3.3 discusses the calculation of the stoichiometric $m_{\mathrm{air}}/m_{\mathrm{biomass}}$ ratio based on measured elemental composition and assuming the partial oxidation reaction.

(d) Total gas yield (wt %) was estimated by calculating the tar and char product weight percent of the feed biomass mass.

$$\begin{aligned}&\mathrm{total\ gas\ (wt\ \%)} = 100\ \mathrm{wt\ \%} - \mathrm{tar(wt\ \%)}\\&\quad - \mathrm{char(wt\ \%)}\end{aligned} \tag{6}$$

(e) The carbon conversion is the molar ratio of carbon (C) output to that of input, thus the gasification efficiency was reflected by the carbon conversion, where the elemental balance method was employed and was calculated by eq 7.

$$\begin{aligned}&\mathrm{carbon\ conversion\ efficiency\ (CCE)}\\&= \frac{\mathrm{total\ mol\ of\ carbon\ output}}{\mathrm{total\ mol\ of\ carbon\ input}} \times 100\end{aligned} \tag{7}$$

2.8. Kinetic Modeling Applied to TGA and DTG Curves. Kinetic modeling theory of solid−gas reactions was applied to the TGA and DTG curve to simulate the gasification of the dried microalgae powder under air flow.

Based on the DTG curve which showed five peaks, the TGA curve was discretized into three zones (I, II, III), with the second zone featuring three subzones (II(i), II(ii), and II(iii)). Each zone and subzone was characterized by a range of temperatures and conversions, and model fitting was carried out individually for each zone and subzone. A range of models were tested according to Khawam and Flannagan's review[31] on solid state kinetic models. Goodness of fit was assessed on minimization of the sum of the relative errors between experimental conversions and modeled conversions. Conversion in each zone and subzone was defined by

$$\alpha_i^* = \frac{\alpha_{\mathrm{max},i} - \alpha_i}{\alpha_{\mathrm{max},i} - \alpha_{\mathrm{min},i}} \tag{8}$$

where i represents the subzone for which the fit was carried out and α_{max} and α_{min} are the maximum and minimum mass loss fractions delimiting the zone for the fit. Thus, experimental conversion α_i^* was always bounded between 0 and 1. A best fit model was then found for α_i^* using model equations, and then a modeled mass loss fraction α_i could then be recalculated from the knowledge of the limiting mass loss fractions for the zone tested.

The models that were found to best fit the identified subzones were the following:

DOI: 10.1021/acs.energyfuels.6b03468
Energy Fuels 2017, 31, 2959−2969

Avrami−Erofeyev AN: "A2" and "A3"

$$\alpha_i^* = 1 - \exp(-(k \times t)^N)$$

Avrami−Erofeyev models represent nucleation and nuclei growth, with the "N" value indicating the dimension of the nuclei, $N = 2$ means 2D nuclei, i.e., disc shape, $N = 3$ means 3D nuclei, e.g. spherical shape.

Contracting surface

$$\alpha_i^* = 1 - (1 - (k \times t))^2$$

Contracting volume

$$\alpha_i^* = 1 - (1 - (k \times t))^3$$

zero-order

$$\alpha_i^* = k \times t$$

In the above equations, the rate constant k follows the Arrhenius expression:

$$k = A \times \exp\left(-\frac{E}{RT}\right) \quad (9)$$

where A is the pre-exponential factor and E is the apparent activation energy of the reaction taking place. Time t is related to absolute temperature T via the TGA's heating rate β and the initial temperature T_0 in kelvin:

$$(T - T_0) = \beta \times t \quad (10)$$

Comparisons modeled and experimentally obtained α_i, vs T, and between modeled and experimentally obtained DTG curves ($d\alpha_i/dt$) vs T were then performed.

3. RESULTS AND DISCUSSION

3.1. Thermal Decomposition Behavior of Microalgal Biomass from TGA Experiments. The TG (weight loss vs temperature) and DTG (rate of weight loss vs temperature) profiles of *Chlorella vulgaris* biomass under 10 and 20 °C min^{-1} heating rates are presented in Figure 2. Referring to DTG curves in Figure 2, it can be seen that the gasification behavior of the microalgae is a complex process where the decomposition process is categorized into three zones.

The first zone (I) appeared below 150 °C, which is recognized as the elimination of the cellular water. The maximum weight loss was witnessed in the second zone (II), which covers the pyrolytic temperature, indicating the devolatilization of soluble polysaccharides and proteins followed by lipids composition. This resulted in the production of the volatile and char formation.[32] The weight loss behavior of the third zone (III) in the presence of elevated temperature is distinguished by a negligible weight loss, which is perhaps caused by the breakdown of insoluble polysaccharides and crude lipids followed by carbonaceous residuals retained in char residues. More than 80% of the weight loss was attained at the second zone (II) under both heating rates (10 and 20 °C min^{-1}). However, different feedstocks have different combustion behavior, which can be primarily attributed to the strength of cross-links between carbohydrates, protein, lipids, and lignin.[33]

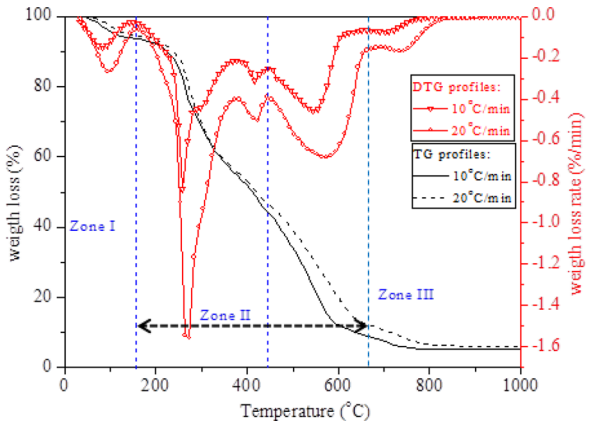

Figure 2. TG and DTG profiles of the microalgal biomass gasification at 10 and 20 °C min^{-1} heating rates.

However, the DTG profiles of zones II and III for both heating rates are complex due to the various peaks (Figure 2). Thus, zones II and III are further classified in this study to understand the complexity of microalgae gasification. The mechanism of both zones (II and III) can be divided into four events as below:

$$\mathrm{B} \rightarrow \begin{cases} \text{component 1} \xrightarrow[\text{reaction 1}]{k_1} \text{gas} + \text{char} \\ \text{component2} \xrightarrow[\text{reaction 2}]{k_2} \text{gas} + \text{char} \\ \text{component 3} \xrightarrow[\text{reaction 3}]{k_3} \text{gas} + \text{char} \end{cases}$$

$$\text{char} + \mathrm{O_2} \xrightarrow[\text{reaction 4}]{k_4} \text{ash} + \mathrm{CO_2}$$

where B denotes biomass.

3.2. Kinetic Modeling of Zones I, II, and III. Table 1 lists the boundaries chosen to model the TGA mass loss fraction and its DTG curve for the experiment performed with the heating rate 20 °C min^{-1} and shows the best models used to fit the mass loss fraction zone by zone, together with their corresponding Arrhenius parameters.

Closeness of the models with the mass loss fraction measured in the TGA experiment and with their DTG curves are shown in Figure 3.

Two models were found to provide a best fit for zone II(i): A3 and contracting volume. Arrhenius parameters are very dependent upon the model chosen to fit the data. For a same data set like that of zone II(i), values of A and E were several orders of magnitude higher for the contracting volume model than for Avrami−Erofeyev's A3. Zones I, II(iii), and III resulted in excellent fits, while zones II(i) and II(ii) incurred slight errors in the DTG curves, which were subsequently negligible when integrated in the TGA's fraction of mass loss curve. Numerous kinetic studies of the pyrolysis of microalgae have been conducted for experiments under N_2 flow. These most often assumed an nth-order reaction scheme for different temperature zones.[31,32,34] As a result, the derived activation energies were typically in the 40−100 kJ mol^{-1} range. In the TGA experiments carried under air flow of the present study, an nth order reaction scheme yielded poorer fits than those ultimately chosen.

3.3. Ultimate Analysis, Enthalpy of Formation, and Calorific Value of the Microalgae. Table 2 shows the elemental composition, calorific value, molar formula and density of the sampled *C. vulgaris*.

DOI: 10.1021/acs.energyfuels.6b03468
Energy Fuels 2017, 31, 2959−2969

Table 1. Kinetic Model Fitting of *C. vulgaris* from TGA-DTG Experiments via a Range of Models

zone	T_{min} (°C)	α min	T_{max} (°C)	α max	model	A (s^{-1})	E (kJ mol^{-1})
I	36	1.00	176	0.94	A2	0.0133	3.6
II(i)	165	0.94	367	0.59	A3	0.0040	2.0
II(i)	165	0.94	367	0.59	contracting volume	3.9981	41.0
II(ii)	358	0.60	468	0.45	zero-order	0.0037	1.1
II(iii)	458	0.47	677	0.12	contracting surface	0.0407	26.3
III	649	0.13	833	0.06	Contracting surface	0.0290	24.7

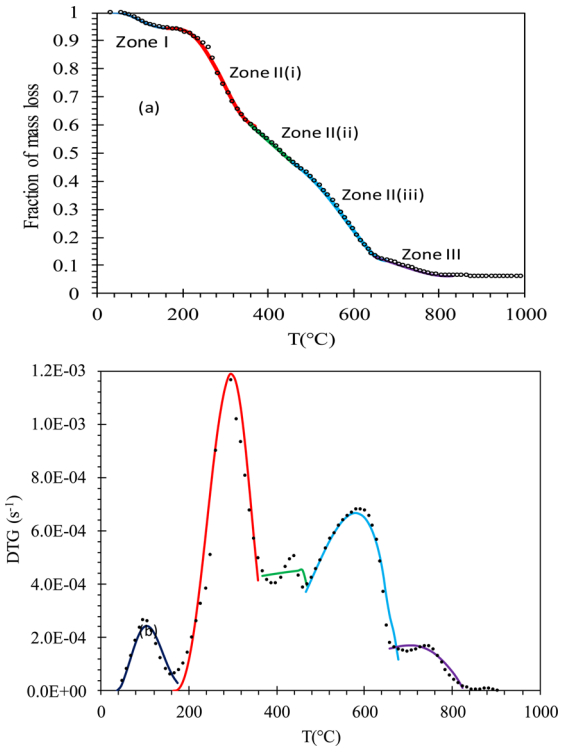

Figure 3. (a) Experimental TG and modeled TG fraction of mass loss vs temperature, (b) experimental DTG, and modeled DTG curves.

The equivalence ratio used to describe the gasification experiments (eq 5) is defined on the basis of the combustion reaction (COM):

$$C_1H_{1.418}O_{0.339}N_{0.251}S_{0.045} + 1.481O_2 \rightarrow CO_2 + 0.709H_2O + 0.251NO_2 + 0.045SO_2$$

With a corresponding molar mass of 23.83 g mol^{-1} and assuming a 79 mol % N_2, 21 mol % O_2 composition for air, the stoichiometric air to biomass requirement $(m_{air}/m_{biomass})_{stoichiometric}$ was therefore 8.54.

With the higher calorific value of 22.19 MJ kg^{-1} determined using methodology described in section 2.2, a value of −65.7 kJ mol^{-1} was derived for the enthalpy of formation of the *C. vulgaris* biomass sample when defined as $C_1H_{1.418}O_{0.339}N_{0.25}S_{0.045}$. Subsequently the gasification reactions of significance involving the biomass reactant (neglecting the fate of N and S) would have incurred the following enthalpies of reaction at 298 K in kilojoules per mole of biomass:

Partial oxidation (POX)

$$C_1H_{1.418}O_{0.339} + 0.330O_2 \rightarrow CO + 0.709H_2 \quad \Delta H_{POX} = -44.9\ kJ\ mol_{bio}^{-1} \tag{11}$$

Combustion (COM)

$$C_1H_{1.418}O_{0.339} + 1.185O_2 \rightarrow CO_2 + 0.709H_2O_{(G)} \quad \Delta H_{COM} = -499.3\ kJ\ mol_{bio}^{-1} \tag{12}$$

Methanation (MTH)

$$C_1H_{1.418}O_{0.339} + 0.476H_2O_{(G)} \rightarrow 0.592CH_4 + 0.408CO_2 \quad \Delta H_{MTH} = -24.0\ kJ\ mol_{bio}^{-1} \tag{13}$$

Thermal decomposition (TD)

$$C_1H_{1.418}O_{0.339} \rightarrow C_{(S)} + 0.370H_2 + 0.339H_2O_{(G)} \quad \Delta H_{TD} = -16.4\ kJ\ mol_{bio}^{-1} \tag{14}$$

Steam gasification (STG)

$$C_1H_{1.418}O_{0.339} + 0.661H_2O_{(G)} \rightarrow CO + 1.37H_2 \quad \Delta H_{STG} = +114.9\ kJ\ mol_{bio}^{-1} \tag{15}$$

3.4. Effect of Biomass Loading on Product Distribution and Syngas Composition from HQR Experiments.

The microalgae gasification process initiates with dehydration, then pyrolysis or devolatilization and ends up with oxidation or combustion. During the gasification process, biomass is first dried and pyrolyzed to volatile gases, biochar, and tar. The pyrolyzed gases of steam-rich atmosphere change into permanent syngas by reacting with gasifying agent at higher temperatures. In addition to eqs 11−15, the mechanism of gasification might be described by the following reactions as shown in eqs 16−23:

Microalgal biomass gasification

$$C_xH_yO_z + \text{heat} \rightarrow \text{steam} + \text{biochar} + \text{syngas}(H_2, CO, CO_2, CH_4, C_nH_m) + \text{tar} + \text{char} \tag{16}$$

Oxidation reaction 1

$$C(\text{char}) + 1/2O_2 \rightarrow CO \quad -111\ kJ\ mol_C^{-1} \tag{17}$$

Table 2. Elemental Composition and Calorific Value of Sampled *C. vulgaris*

C (wt %)	H (wt %)	N (wt %)	S (wt %)	O (wt %)	HHV (MJ kg^{-1})	molar formula C1 basis
50.39 ± 1.6	6.01 ± 0.7	14.77 ± 3.3	6.05 ± 0.5	22.78 ± 7.2	22.19	$C_1H_{1.418}O_{0.339}N_{0.251}S_{0.045}$

DOI: 10.1021/acs.energyfuels.6b03468
Energy Fuels 2017, 31, 2959−2969

Oxidation reaction 2

$$C(char) + O_2 \rightarrow CO_2 \quad -393\ kJ\ mol_C^{-1} \tag{18}$$

Water−gas reaction

$$C(char) + H_2O \leftrightarrows H_2 + CO \quad +131\ kJ\ mol_C^{-1} \tag{19}$$

Reverse Boudouard (RB)

$$C(char) + CO_2 \leftrightarrows 2CO \quad +172\ kJ\ mol_C^{-1} \tag{20}$$

Methanation reaction 2

$$C(char) + 2H_2 \leftrightarrows CH_4 \quad -75\ kJ\ mol_C^{-1} \tag{21}$$

Water−gas shift (WGS) reaction

$$CO + H_2O \leftrightarrows H_2 + CO_2 \quad -41.2\ kJ\ mol_{CO}^{-1} \tag{22}$$

Methane steam reforming reaction

$$CH_4 + H_2O \leftrightarrows CO + 3H_2 \quad +206\ kJ\ mol_{CH4}^{-1} \tag{23}$$

The effect of products distribution (i.e., gas, tar, ash) and syngas production at different microalgal biomass concentrations are presented in Table 3 and Figure 4. The biomass loading is an influential parameter, and it is important to find the optimum point in the conversion process since increase in biomass loading does not always favor the H_2 production.[35] Figure 4a represents the product distribution achieved by varying the microalgal biomass loading while the temperature, ER, heating rate, and holding time were kept constant at 700 °C, 0.26, 10 °C min^{-1}, and 20 min, respectively. The gas yields gradually decreased from 78.6 to 66.6 wt %, when the biomass concentrations were increased from 0.3 to 2 g (Table 3). On the other hand, char and tar yields increased from 9.8 to 18.1 and 11.6 to 15.3 wt %. The increase in char and tar compositions and decrease in overall gas yield were due to the lower gasification temperature and lower ER in reactor.[29] Although, the char and tar contents were high in this work, the compostion of tar was found lower compared to that of hydrothermal liquefaction.[34−37] Anastasakis et al.[38] found that the highest tar yield was 19.5 wt % when gasifying *Saccharina* (brown algae), while the maximum tar yield of 15.3 wt % was obtained in this work.

Table 3. Summary of Operating Conditions and Results for the Different Biomass Loadings in Microalgae (*C. vulgaris*) Gasification

	operating parameters					AV[a]
gasification agent			air			
temperature (°C)			700			
ER			0.26			
heating rate (°C min^{-1})			10			
holding time (min)			20			
microalgal biomass loading (g)	0.3	0.6	1	1.5	2	1.08
char (wt %)	9.7	10.4	11.6	15.5	18.1	13.0
tar (wt %)	11.6	12.5	12.6	13.3	15.3	13.0
total gas (wt %)	78.6	77.1	75.8	71.1	66.6	73.8
H_2 (vol %)	13.1	18.1	24.2	20.5	19.5	19.1
CO (vol %)	26.0	24.4	22.7	20.4	21.3	22.9
CH_4 (vol %)	13.2	15.9	17.4	22.8	24.3	18.7
CO_2 (vol %)	47.6	41.4	38.6	32.1	26.7	37.3
H_2 yield (mg g $syngas^{-1}$)	0.068	0.010	0.013	0.012	0.011	0.010
CCE (%)	53.1	53.7	53.4	53.3	53.2	52.9
LHV (MJ N m^{-3})	9.4	10.7	11.7	12.9	13.5	11.6
H_2/CO	0.5	0.7	1.06	1.0	0.91	0.8

[a]Average values.

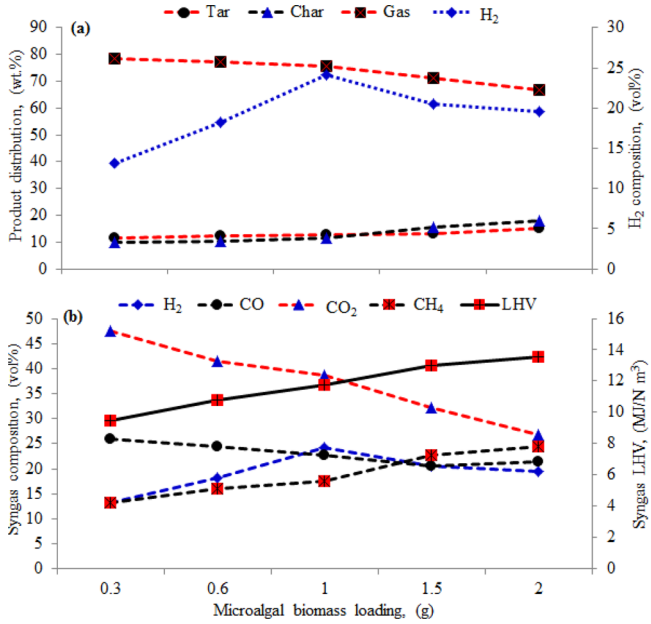

Figure 4. Effect of microalgal biomass loading concentrations. (a) Product distribution. (b) Product gas composition. Temperature 700 °C; ER 0.26; heating rate 10 °C min^{-1}; holding time 20 min.

Figure 4b shows the that maximum syngas fractions achieved were 24.20 and 26 vol % for H_2 and CO at 1 and 0.3 g, respectively. H_2 showed a decreasing trend, when biomass loading was increased from 1 g. This can be justified by the fact that the increasing biomass loading contributed to less residence time per volume of air, which may trigger less oxygen to be in contact with the biomass particles.[39] Thus, the decreased heat transfer due to increasing biomass loading resulted in less volatile gas production in pyrolysis zone and subsequently reducing the gasification process, where the biomass sample remained raw or incompletely gasified. The partially gasified/leftover samples trend during the gasification process can be observed from the results shown in Table 3. In addition, CH_4 content had a positive trend from 13.24 to 24.39 vol % and CO_2 contents dramatically decreased from 47.6 to 26.75 vol %, due to the reactions in eqs 20 and 23. The obtained results are in agreement with the study conducted by Seo et al.[40] where H_2 and CH_4 were found increased due to the increase in biomass loading. According to Table 3, the highest H_2 yield was achieved at 0.013 mg g $syngas^{-1}$, while the highest CCE was achieved at 53.7%. The LHV of syngas was increased in the range of biomass loading to 13.53 MJ N m^{-3}. The H_2/CO ratio was increased from 0.50 to 1.06 with the biomass loading from 0.3 to 1 g. Pan et al.[41] gasified the blended biomass/coal and reported that the increasing biomass ratio in gasifier increased the intensity of the overall gas yield and its heating value. In our HQR experiments, the microalgal biomass loading of 1 g contributed to the highest H_2 production.

DOI: 10.1021/acs.energyfuels.6b03468
Energy Fuels 2017, 31, 2959−2969

Table 4. Summary of Operating Conditions and Results Obtained at Different Temperatures in Microalgae (*C. vulgaris*) Gasification

	operating parameters						AV[a]
gasification agent	air						
biomass loading (g)	1.0						
ER	0.26						
heating rate (°C min^{-1})	10						
holding time (min)	20						
reactor temperature (°C)	700	750	800	850	900	950	825
char (wt %)	27.1	25.6	23.3	19.3	17.4	13.5	21.0
tar (wt %)	18.4	15.6	14.0	12.2	11.0	10.4	13.6
total gas (wt %)	54.6	58.7	62.5	68.4	71.5	76.1	65.3
H_2 (vol %)	22.5	25.7	28.8	33.2	35.1	39.2	30.7
CO (vol %)	20.6	23.4	24.7	29.8	25.5	22.4	24.4
CH_4 (vol %)	21.4	20.2	19.9	18.4	18.2	17.4	19.2
CO_2 (vol %)	30.8	29.6	28.9	26.9	26.4	25.2	27.9
H_2 yield (mg g $syngas^{-1}$)	0.010	0.013	0.015	0.019	0.022	0.028	0.017
CCE (%)	40.8	43.9	46.8	51.9	53.4	56.3	48.8
LHV (MJ N m^{-3})	12.6	12.9	13.4	13.9	13.5	13.1	13.2
H_2/CO	1.1	1.0	1.1	1.1	1.3	1.7	1.2

[a]Average values.

Therefore, 1 g of microalgal biomass loading was chosen to be used for further experiments.

3.5. Effect of Temperature on Product Distribution and Syngas Composition. Temperature remains the most important parameter affecting the overall biomass conversion with major influence on the final product compositions. The fundamental role of temperature is to supply heat of decomposition to break the bonding structure of the feedstock as well as providing more thermodynamically favorable conditions for the endothermic gasification reactions such as steam reforming, reverse Boudouard, and char and tar gasification to CO and H_2 products as opposed to CH_4 product. The profile of product composition with reactor temperature quantifies the ability of temperature to decompose the feedstock. To verify the significance of the temperature on the product distributions (i.e., gas, tar, ash) and gas composition, a series of experiments ranging from 700 to 950 °C were performed, and the results are presented in Table 4 and Figure 5.

According to Table 4 and Figure 5a, the total gas and H_2 yield increased from 54.6 to 76.1 wt % and 0.010 to 0.028 mg g $syngas^{-1}$ with increasing temperature from 700 to 950 °C, while char and tar products decreased gradually indicating the significant role of temperature in biomass decomposition and gas formation reactions. This trend might be due to the contribution of secondary reactions such as steam reforming and shifting reactions (eqs 22 and 23). The reactions enhance the production of incondensable gases including H_2 at elevated temperatures and subsequently improve the total yield of syngas.[42−44] There could be various reasons for the increasing total gas yield with reaction temperature, such as (i) higher occurrence of volatile gases in the early pyrolysis stage, which has a higher rate at elevated temperature, (ii) the strengthening of endothermic char gasification reactions, which are advantageous at higher reactor temperatures, and (iii) the increased gaseous products are the result of the cracking and reforming phenomena of heavier hydrocarbons and tars.

According to Figure 5b, the produced gases are H_2, CO, CO_2, CH_4, and some minor species such as C_2H_4 and C_2H_6. The temperature also exhibited great influence by enhancing

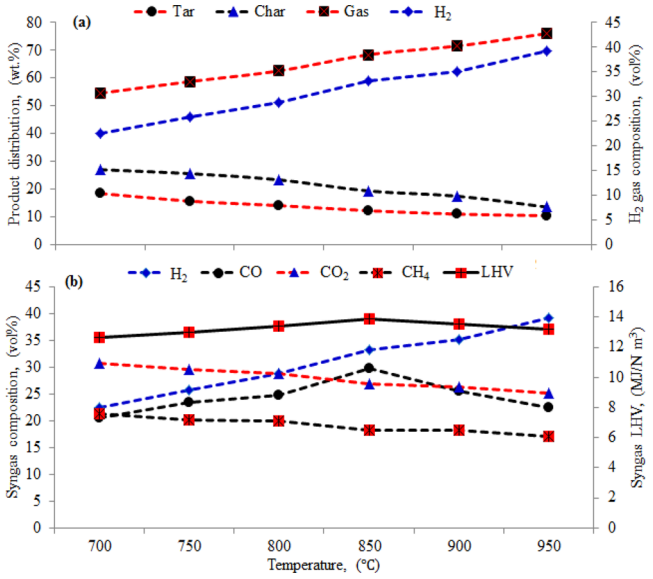

Figure 5. Effect of reaction temperature. (a) Product distrubition. (b) Product gas composition. Biomass loading 1 g; ER 0.26; heating rate 10 °C min^{-1}; holding time 20 min.

syngas production to a maximum fraction of 39.2 and 29.8 vol % for H_2 and CO, respectively. The H_2 production was increased, while the CO_2 and CH_4 production showed an opposite trend with the temperature. The Le Chatelier's principle states that elevated temperatures favor reactants in exothermic reactions and products in endothermic reactions.[44] Thus, the endothermic reactions, such as reverse Boudouard reaction (eq 20), WS reaction (eq 19), steam reforming, and steam reforming of methane (eq 23) are the main dynamics behind the increase of H_2 and CO contents and the decrease of CO_2 and CH_4 compositions.

The CO production was mainly controlled by reverse Boudouard reaction (eq 20). Higher reaction temperature was not favorable for CO production; thus, the concentration of CO decreased from 900 °C onward. According to Figure 5b, CO production was found to be higher below the reactor

DOI: 10.1021/acs.energyfuels.6b03468
Energy Fuels 2017, 31, 2959−2969

temperature of 900 °C. Consequently, the syngas LHV was first intensified and then declined as specified in Table 4.

The decrease in CO content could be due to reverse WG (eq 19) reaction to the right. The overall H_2 production was enhanced at higher temperature, which depends on the balance of three reactions eqs 21−23.[42] WSG reaction always occurs in gasification as a result of the presence of moisture in biomass and water vapor in gasifying agent. The water vapors and CO_2 always promote biomass gasification process.[45] CO_2 and CH_4 concentrations were decreased from 30.8 to 25.2 and 21.4 to 17.4 vol %. The major decrease in the concentration of CO_2 production might be due to reverse boudouard (eq 20) within the range of reaction temperature. The hydrocarbon traces (C_2H_4 and C_2H_6) were comparatively minor and the effect of temperature was insignificant.[46]

Fremaux et al.[44] and Lv et al.[45] reported that higher temperature offers more promising conditions for thermal and steam reforming. In addition, when reaction temperature is strengthened, more carbon conversion in biomass and steam produced during process can be reformed through reactions (eqs 19 and 20). As a result, CCE increased with the increase in temperature as reported in Table 4.

A reduced number of independent, global gasification reactions of the biomass were postulated in order to best describe the yields of char (assumed $C_{(S)}$) and gases obtained in the range of temperatures 800 to 950 °C. The reactions were POX, MTH, TD, RVB, COM, and STG, as defined earlier. The excel solver was then used to match the number of moles of $C_1H_{1.418}O_{0.339}$ biomass that underwent these reactions and the number of $C_{(S)}$ moles reacting via RVB which collectively generated the yields of CO, H_2, CH_4, CO_2, and $C_{(S)}$ observed experimentally. Close to exact matches were found for the molar amounts plotted in Figure 6.

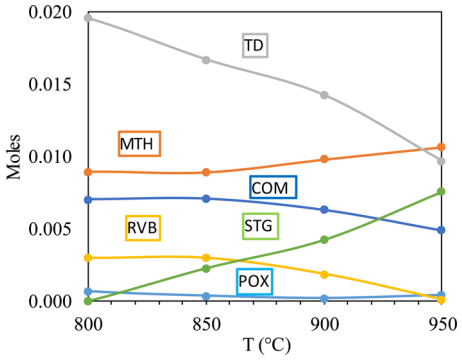

Figure 6. Molar amounts found to undergo the independent reactions MTH, TD, RVB, COM, and STG to match the measured temperature profiles of the molar yields of CO, H_2, CH_4, CO_2, and $C_{(S)}$ in the 800−950 °C range.

Note the matches for 700 and 750 °C (not shown) yielded small negative molar flows for the steam gasification reaction (−0.004 and −0.002, respectively), which indicated that a more detailed set of reactions would have been necessary for these lower temperatures.

As expected, the sharp rising profile of the biomass steam gasification reaction with temperatures confirms the role played by combustion in generating the required steam and contributing to local high temperatures, given the strong endothermicity of STG. It is surprising to see the large roles played both by thermal decomposition and methanation in converting the biomass for all the temperatures, and the underwhelming role played by partial oxidation. According to the molar amounts of biomass reacting attributed to each reaction among the MTH, TD, RVB, COM, and STG set, it was possible to determine the percentage contributions of the relevant reactions to the formation of a particular product. Methane is entirely produced by MTH, but both CO and H_2 had three possible contributors: (RVB, STG, POX) and (TD, STG, POX) respectively. The profiles with temperature of the percentage contributions are shown in Figure 7a and b.

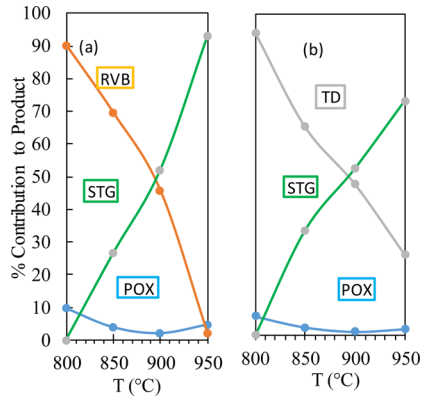

Figure 7. Percentage contribution of global gasification reactions to the formation of product (a) CO and (b) H_2.

According to Figure 7, both CO and H_2 saw a dramatic switch among their main formation reactions when temperatures increased from 800 to 950 °C, both starting with a nil steam gasification contribution and ending with the same reaction becoming clearly dominant. For both species, partial oxidation was negligible. Given that the demand of steam for the STG reaction is 0.66 per mol of $C_1H_{1.418}O_{0.339}$ biomass, the role of combustion of the biomass, responsible for approximately 40−60% of the biomass's consumption, in providing this steam cannot be understated. The dominance of the combustion/steam gasification in generating syngas to the detriment of partial oxidation may be partially explained by the strong negative standard ΔG (change in free Gibbs energy) of the biomass combustion reaction compared to that of its partial oxidation. Although the entropy of formation and specific heat of the microalgae biomass are unknown, educated guesses would place $S_{f,298}$ between 0 and, conservatively, 50 J mol K^{-1}, given its elemental composition and solid state. This would attribute $\Delta G_{298\ K}$ of −516 to −530 kJ mol^{-1} for COM compared to −96 to −111 kJ mol^{-1} for POX, clearly favoring thermodynamically combustion over partial oxidation for the same reactants of microalgal biomass and oxygen.

Knowledge of how the global reactions are interdependent on each other may provide insight into designing more performant reactors. In the absence of catalyst, consumption of the oxygen reactant is more likely to be via complete oxidation rather than partial oxidation, which has significant implications on both the fate of both the N and S contents of the biomass, neglected hitherto in this reaction analysis. Local high temperatures generated by the biomass combustion will potentially be conducive to generation of nitrogen oxides and sulfur dioxides. But the presence of a catalyst in the reactor could possibly ensure the syngas production with a more active partial oxidation, thereby maintaining reducing conditions and milder temperatures evenly in the reactor, potentially

DOI: 10.1021/acs.energyfuels.6b03468
Energy Fuels 2017, 31, 2959−2969

generating N_2 and S_{2-8} instead. The tendency of elevated reaction temperature supporting syngas production has been extensively reported.[30,47,48] LHV of syngas was improved gradually from 12.68 to 13.92 MJ N m^{-3} from 700 to 850 °C. However, LHV of 13.92 MJ N m^{-3} obtained from microalgae gasification is appropriate to be considered as a medium level of heating value for syngas fuel that can be directly utilized for gas turbines, gas engines, or boilers to produce steam for electricity generation. Additionally, it can be used for various chemical industries to form different types of chemicals such as methanol (CH_3OH). The H_2/CO ratio increased from 1.09 to 1.74 with the temperature from 700 to 950 °C. Based on the findings, a conclusion could be drawn that higher temperature (950 °C) is the main reaction temperature of interest for microalgal gasification for our reactor experimental conditions system.

3.6. Effect of Equivalence Ratio (ER) on Product Distribution and Syngas Composition. In the present study, the influence of ER on product distributions and syngas from microalgae gasification was investigated. The ER varied from 0.1 to 0.35 through changes in the air flow rate, while other conditions were held constant. The experimental results are reported in Table 5 and Figure 8. The gas yield was increased from 72.1 to 80.8 wt %, while tar and char were slightly decreased by increasing ER from 0.1 to 0.35.

Table 5. Summary of Operating Conditions and Results Obtained at Different ER in Microalgae (*C. vulgaris*) Gasification

	operating parameters					AV[a]
gasification agent			air			
biomass loading (g)			1.0			
heating rate (°C min^{-1})			10			
temperature (°C)			950			
ER	0.1	0.2	0.26	0.3	0.35	0.24
char (wt %)	15.5	14.8	14.1	13.7	12.3	14.1
tar (wt %)	12.3	10.5	8.7	7.2	6.8	9.1
total gas (wt %)	72.1	74.6	77.1	79.0	80.8	76.7
H_2 (vol %)	13.7	24.7	28.7	23.4	25.5	23.2
CO (vol %)	20.5	21.7	26.7	24.7	19.1	22.5
CH_4 (vol %)	17.7	18.3	19.5	15.7	14.3	17.1
CO_2 (vol %)	27.7	31.6	30.2	33.5	38.6	32.3
H_2 yield (mg g $syngas^{-1}$)	0.009	0.015	0.018	0.015	0.016	0.015
CCE (%)	53.8	54.4	57.4	56.4	55.1	55.4
LHV (MJ N m^{-3})	10.4	11.9	13.4	11.3	10.3	11.4
H_2/CO	0.6	1.1	1.0	0.9	1.3	1.0

[a]Average value.

The ER not only signifies the amount of oxygen injected into the reactor but also affects the gasification temperature under the condition of autothermal operation.[45] On one side, lower ER represents less oxygen into the system, which is not favorable to achieve the gasification reaction equilibrium. Besides, higher ER represents higher gasification temperatures, which promotes the gasification reactions, thereby improves the syngas characteristic to a particular limit. Thus, the gas constituents were affected by the two ambiguous dynamics of ER. Table 5 and Figure 8b shows the experimental output responses that could be distributed into two sections to be examined. First, ER was differed from 0.1 to 0.26 and during the second from 0.26 to 0.35.

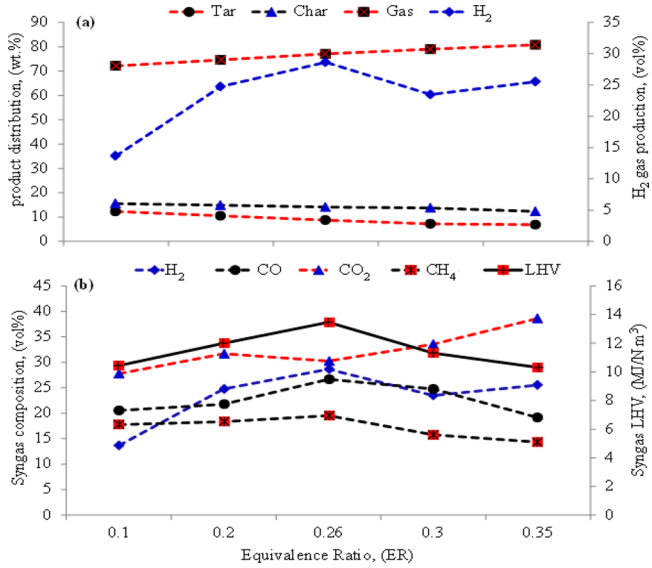

Figure 8. Effect of equivalence ratio (ER). (a) Product distrubition. (b) Product gas composition. Reaction temperature 950 °C; biomass loading 1 g; heating rate 10 °C min^{-1}; holding time 20 min.

In the first phase, the positive effect of ER played a crucial role with respect to H_2, CO, H_2 yield, CCE, and LHV where the yield of those compounds increased from 13.7 to 28.7 vol %, 20.5 to 26.7 vol %, 0.009 to 0.018 mg g $syngas^{-1}$, 53.8% to 57.4%, and 10.4 to 13.4 MJ N m^{-3}. Xiao et al.[49] found that the increasing content of H_2 and CO could be due to the thermal cracking of hydrocarbons at elevated temperatures. During the first section, reaction eq 17 was more likely to occur than reaction eq 18 due to oxygen deficiency. It is shown that reaction eq 7 utilizes 1 mol more carbon than reaction eq 18. As a result, CCE is enhanced with the ER in the first phase. Reasonably, the gasification temperature is augmented with escalating ER.

During the second phase of ER varing from 0.26 to 0.35, the syngas gas (H_2 and CO), H_2 yield, CCE, and LHV of syngas were reduced due to the increased oxidation reactions of combustible product gases as stated in Table 5, causing a large increase in CO_2 concentration.

From the experimental result of varying ER, it can be concluded that a moderate ER is required for microalgal biomass gasification. The lower ER will lower down the oxygen quantity into the system, which is not advantageous to attain reaction equilibrium in enhancing the syngas concentrations. The increase in ER will consume more H_2 and other gases due to oxidation reaction. In this research, the optimum value of ER was 0.26 as shown in Table 5.

4. CONCLUSION

Thermogravimetric features were considered and four solid state kinetic models have been found suitable to simulate the air gasification of microalgae biomass. The differential thermogravimetric analysis (DTG) was categorized into three zones: (I) dehydration; (II) devolatilization of soluble polysaccharides and proteins followed by lipids; (III) degradation of carbonaceous residual. Zone II presents three subzones (II(i), II(ii), and II(iii)) and more than 80% of the weight loss under both heating rates (10 and 20 °C min^{-1}). The kinetic parameters

DOI: 10.1021/acs.energyfuels.6b03468
Energy Fuels 2017, 31, 2959−2969

derived from thermogravimetric data are within the acceptable range in comparison with the literatures. The investigated parameters and their synergistic results using HQR, provide the valuable information for high syngas production. Among the examined parameters temperature was found to be the most significant parameter influencing all chemical reactions involved in the gasification process, 950 °C being the optimum for gasification in the HQR. According to the range of microalgal biomass loading from 0.3 to 2 g, 1 g of biomass loading was found to be an optimal value of higher H_2 production for our HQR reactor. ER had multifaceted influences on experimental findings, which varies according to set operation conditions. In the current study, the optimum value of ER was found to be 0.26. The microalgae biomass demonstrated several valuable characteristics for future bioenergy research in relation to high syngas production. An integrated process system including different type of catalyst usage can be efficiently applied for high quality syngas production. Relating the results with other published papers, it is expected that HQR dry air-gasification of microalgae biomass with additional process description will play a significant role in future designs of commercial scale applications.

AUTHOR INFORMATION

Corresponding Authors

*Tel.: +86 10 62784701. E-mail: ming.zhao@tsinghua.edu.cn (M.Z.).

*E-mail: mh_razif@upm.edu.my (R.H.).

ORCID

Ming Zhao: 0000-0002-5801-5593

Notes

The authors declare no competing financial interest.

ACKNOWLEDGMENTS

M.Z. thanks the National Recruitment Program of Global Youth Experts (The National Youth 1000−Talent Program) of China (grant number: 20151710227) and the Tsinghua University Initiative Scientific Research Program (grant number: 20161080094) for support. R.H. thanks the Ministry of Higher Education (MOHE) Fundamental Research Grant Scheme (Project Code: 03-02-13-1297FR) and the Department of Chemical and Environmental Engineering, Universiti Putra Malaysia, for support. V. Dupont's contribution acknowledges the support of the Global Challenge Research Fund (GCRF) Institutional EPSRC Grant to The University of Leeds, UK, through RCUK's grant EP/P51097X/1. Data used to make figures and tables for this paper can be found at http://doi.org/10.5518/165.

REFERENCES

(1) Yoon, S. J.; Choi, Y. C.; Son, Y. I.; Lee, S. H.; Lee, J. G. Gasification of biodiesel by-product with air or oxygen to make syngas. *Bioresour. Technol.* **2010**, *101*, 1227−1232.

(2) Guoxin, H.; Hao, H. Hydrogen rich fuel gas production by gasification of wet biomass using a CO_2 sorbent. *Biomass Bioenergy* **2009**, *33*, 899−906.

(3) Dunn, S. Hydrogen futures: toward a sustainable energy system. *Int. J. Hydrogen Energy* **2002**, *27*, 235−64.

(4) Florin, N. H.; Harris, A. T. Hydrogen production from biomass coupled with carbon dioxide capture: the implications of thermodynamic equilibrium. *Int. J. Hydrogen Energy* **2007**, *32*, 4119−34.

(5) Martavaltzi, C. S.; Lemonidou, A. A. Hydrogen production via sorption enhanced reforming of methane: Development of a novel hybrid material—reforming catalyst and CO_2 sorbent. *Chem. Eng. Sci.* **2010**, *65*, 4134−40.

(6) IEA Bioenergy. *A sustainable and reliable energy source*; International Energy Agency: Paris, 2009.

(7) Popp, J.; Lakner, Z.; Harangi-Rákos, M.; Fári, M. The effect of bioenergy expansion: food, energy, and environment. *Renewable Sustainable Energy Rev.* **2014**, *32*, 559−578.

(8) Cherry, R. S. A hydrogen utopia? *Int. J. Hydrogen Energy* **2004**, *29*, 125−129.

(9) Nigam, P. S.; Singh, A. Production of liquid biofuels from renewable resources. *Prog. Energy Combust. Sci.* **2011**, *37*, 52−68.

(10) McKendry, P. Energy production from biomass (part 1): overview of biomass. *Bioresour. Technol.* **2002**, *83*, 37−46.

(11) Maddi, B.; Viamajala, S.; Varanasi, S. Comparative study of pyrolysis of algal biomass from natural lake blooms with lignocellulosic biomass. *Bioresour. Technol.* **2011**, *102*, 11018−26.

(12) Skorupskaite, V.; Makareviciene, V.; Levisauskas, D. Optimization of mixotrophic cultivation of microalgae Chlorella sp. for biofuel production using response surface methodology. *Algal Res.* **2015**, *7*, 45−50.

(13) Clarens, A. F.; Resurreccion, E. P.; White, M. A.; Colosi, L. M. Environmental life cycle comparison of algae to other bioenergy feedstocks. *Environ. Sci. Technol.* **2010**, *44*, 1813−9.

(14) Chen, P.; Xie, Q.; Addy, M.; Zhou, W.; Liu, Y.; Wang, Y.; Ruan, R.; et al. Utilization of municipal solid and liquid wastes for bioenergy and bio products production. *Bioresour. Technol.* **2016**, *215*, 163−172.

(15) van Steen, E.; Claeys, M. Fischer−Tropsch Catalysts for the Biomass-to-Liquid (BTL) Process. *Chem. Eng. Technol.* **2008**, *31*, 655−66.

(16) Patzelt, D. J.; Hindersin, S.; Elsayed, S.; Boukis, N.; Kerner, M.; Hanelt, D. Hydrothermal gasification of Acutodesmus obliquus for renewable energy production and nutrient recycling of microalgal mass cultures. *J. Appl. Phycol.* **2015**, *27*, 2239−50.

(17) Cherad, R.; Onwudili, J. A.; Biller, P.; Williams, P. T.; Ross, A. B. Hydrogen production from the catalytic supercritical water gasification of process water generated from hydrothermal liquefaction of microalgae. *Fuel* **2016**, *166*, 24−8.

(18) Tiong, L.; Komiyama, M.; Uemura, Y.; Nguyen, T. T. Catalytic supercritical water gasification of microalgae: Comparison of Chlorella vulgaris and Scenedesmus quadricauda. *J. Supercrit. Fluids* **2016**, *107*, 408−13.

(19) Stucki, S.; Vogel, F.; Ludwig, C.; Haiduc, A. G.; Brandenberger, M. Catalytic gasification of algae in supercritical water for biofuel production and carbon capture. *Energy Environ. Sci.* **2009**, *2*, 535−41.

(20) Hirano, A.; Hon-Nami, K.; Kunito, S.; Hada, M.; Ogushi, Y. Temperature effect on continuous gasification of microalgal biomass: theoretical yield of methanol production and its energy balance. *Catal. Today* **1998**, *45*, 399−4.

(21) Minowa, T.; Yokoyama, S. Y.; Kishimoto, M.; Okakura, T. Oil production from algal cells of Dunaliella tertiolecta by direct thermochemical liquefaction. *Fuel* **1995**, *74*, 1735−8.

(22) Alghurabie, I. K.; Hasan, B. O.; Jackson, B.; Kosminski, A.; Ashman, P. J. Fluidized bed gasification of Kingston coal and marine microalgae in a spouted bed reactor. *Chem. Eng. Res. Des.* **2013**, *91*, 1614−24.

(23) Khoo, H. H.; Koh, C. Y.; Shaik, M. S.; Sharratt, P. N. Bioenergy co-products derived from microalgae biomass via thermochemical conversion−life cycle energy balances and CO_2 emissions. *Bioresour. Technol.* **2013**, *143*, 298−7.

(24) Yang, K. C.; Wu, K. T.; Hsieh, M. H.; Hsu, H. T.; Chen, C. S.; Chen, H. W. Co-gasification of woody biomass and microalgae in a fluidized bed. *J. Taiwan Inst. Chem. Eng.* **2013**, *44*, 1027−33.

(25) Kumar, G. S.; Gupta, A. V.; Viswanadham, D.; Abhiram, M. Advances in gasification technology a basic review. In the *1st international conference on advances in thermal and energy systems*; 2013; pp 53−59.

(26) Hernández, J. J.; Aranda-Almansa, G.; Bula, A. Gasification of biomass wastes in an entrained flow gasifier: effect of the particle size and the residence time. *Fuel Process. Technol.* **2010**, *91*, 681−92.

DOI: 10.1021/acs.energyfuels.6b03468
Energy Fuels 2017, 31, 2959−2969

(27) Zhao, B.; Zhang, X.; Sun, L.; Meng, G.; Chen, L.; Xiaolu, Y. Hydrogen production from biomass combining pyrolysis and the secondary decomposition. *Int. J. Hydrogen Energy* **2010**, *35*, 2606−11.
(28) Raheem, A.; Wakg, W. A.; Yap, Y. T.; Danquah, M. K.; Harun, R. Optimization of the microalgae Chlorella vulgaris for syngas production using central composite design. *RSC Adv.* **2015**, *5*, 71805−15.
(29) Perry, R. H.; Chilton, C H. *Chemical Engineer's Handbook*, 5th ed.; Mcgraw-Hill-Kogakusha: Tokyo, 1973.
(30) Alipour Moghadam, R.; Yusup, S.; Azlina, W.; Nehzati, S.; Tavasoli, A. Investigation on syngas production via biomass conversion through the integration of pyrolysis and air-steam gasification processes. *Energy Convers. Manage.* **2014**, *87*, 670−75.
(31) Khawam, A.; Flanagan, D. R. Solid-state kinetic models: basics and mathematical fundamentals. *J. Phys. Chem. B* **2006**, *110*, 17315−28.
(32) Gai, C.; Zhang, Y.; Chen, W. T.; Zhang, P.; Dong, Y. Thermogravimetric and kinetic analysis of thermal decomposition characteristics of low-lipid microalgae. *Bioresour. Technol.* **2013**, *150*, 139−48.
(33) Pérez, J.; Munoz-Dorado, J.; de la Rubia, T. D.; Martinez, J. Biodegradation and biological treatments of cellulose, hemicellulose and lignin: an overview. *Int. Microbiol.* **2002**, *5*, 53−63.
(34) Shuping, Z.; Yulong, W.; Mingde, Y.; Chun, L.; Junmao, T. Pyrolysis characteristics and kinetics of the marine microalgae Dunaliella tertiolecta using thermogravimetric analyzer. *Bioresour. Technol.* **2010**, *101*, 359−65.
(35) Devi, L.; Ptasinski, K. J.; Janssen, F. J. A review of the primary measures for tar elimination in biomass gasification processes. *Biomass Bioenergy* **2003**, *24*, 125−40.
(36) Vardon, D. R.; Sharma, B. K.; Scott, J.; Yu, G.; Wang, Z.; Schideman, L.; Zhang, Y.; Strathmann, T. J. Chemical properties of bio crude oil from the hydrothermal liquefaction of Spirulina algae, swine manure, and digested anaerobic sludge. *Bioresour. Technol.* **2011**, *102*, 8295−03.
(37) Biller, P.; Ross, A. B. Potential yields and properties of oil from the hydrothermal liquefaction of microalgae with different biochemical content. *Bioresour. Technol.* **2011**, *102*, 215−25.
(38) Anastasakis, K.; Ross, A. B. Hydrothermal liquefaction of the brown macroalga Laminaria saccharina: effect of reaction conditions on product distribution and composition. *Bioresour. Technol.* **2011**, *102*, 4876−83.
(39) Wan Ab Karim Ghani, W. A.; Moghadam, R. A.; Salleh, M. A.; Alias, A. B. Air gasification of agricultural waste in a fluidized bed gasifier: hydrogen production performance. *Energies* **2009**, *2*, 258−8.
(40) Seo, M. W.; Goo, J. H.; Kim, S. D.; Lee, S. H.; Choi, Y. C. Gasification characteristics of coal/biomass blend in a dual circulating fluidized bed reactor. *Energy Fuels* **2010**, *24*, 3108−18.
(41) Pan, Y. G.; Velo, E.; Puigjaner, L. Pyrolysis of blends of biomass with poor coals. *Fuel* **1996**, *75*, 412−18.
(42) Midilli, A.; Dogru, M.; Howarth, C. R.; Ayhan, T. Hydrogen production from hazelnut shell by applying air-blown downdraft gasification technique. *Int. J. Hydrogen Energy* **2001**, *26*, 29−37.
(43) Chen, G.; Andries, J.; Luo, Z.; Spliethoff, H. Biomass pyrolysis/gasification for product gas production: the overall investigation of parametric effects. *Energy Convers. Manage.* **2003**, *44*, 1875−84.
(44) Fremaux, S.; Beheshti, S.; Ghassemi, H.; Shahsavan-Markadeh, R. An experimental study on hydrogen-rich gas production via steam gasification of biomass in a research-scale fluidized bed. *Energy Convers. Manage.* **2015**, *91*, 427−32.
(45) Lv, P. M.; Xiong, Z. H.; Chang, J.; Chen, Y.; Zhu, J. X.; Wu, C. Z. An experimental study on biomass air−steam gasification in a fluidized bed. *Bioresour. Technol.* **2004**, *95*, 95−101.
(46) Xianwen, D.; Chuangzhi, W.; Haibin, L.; Yong, C. Fast pyrolysis of biomass in CFB reactor. *Energy Fuels* **2000**, *14*, 552−7.
(47) Tavasoli, A.; Ahangari, M. G.; Soni, C.; Dalai, A. K. Production of hydrogen and syngas via gasification of the corn and wheat dry distiller grains (DDGS) in a fixed-bed micro reactor. *Fuel Process. Technol.* **2009**, *90*, 472−82.
(48) Supramono, D.; Tristantini, D.; Rahayu, A.; Suwignjo, R. K.; Chendra, D. H. Syngas Production from Lignite Coal Using K_2CO_3 Catalytic Steam Gasification with Controlled Heating Rate in Pyrolysis Step. *Procedia Chem.* **2014**, *9*, 202−9.
(49) Xiao, R.; Jin, B.; Zhou, H.; Zhong, Z.; Zhang, M. Air gasification of polypropylene plastic waste in fluidized bed gasifier. *Energy Convers. Manage.* **2007**, *48*, 778−86.

DOI: 10.1021/acs.energyfuels.6b03468
Energy Fuels 2017, 31, 2959−2969